LIKELIHOOD-BASED IMAGE SEGMENTATION AND CLASSIFICATION: CONCEPTS AND APPLICATIONS

A. A. ABKAR[*], M. A. SHARIFI[**]
Soil Conservation and Watershed Management Research Center (SCWMRC)
P.O. Box 13445-1136, Tehran, Iran
Abkar@itc.nl
[**]International Institute for Aerospace Survey and Earth Sciences (ITC)
P.O. Box 6, 7500 AA Enschede, The Netherlands
Alisharifi@itc.nl

Working Group IC-7

KEY WORDS: Classification, Knowledge Engineering, Remote Sensing, Segmentation.

ABSTRACT

This paper describes a likelihood-based segmentation and classification method for remotely sensed images. It is based on optimization of a utility function, described as a function of likelihood of all objects and their parameters. As the likelihood or posterior probabilities are calculated per object rather than per pixel, the variance in (spectral) likelihoods will be greatly reduced. From a users point of view the result has either a maximum probability for truth (likelihood) or maximum utility (benefit). It includes a new approach for segmentation, which is based on criteria derived from local average likelihoods instead of local means or variances, making the segmentation method much less sensitive to radiometric outliers. Due to these capabilities the method represents a step towards operationalization of remote sensing.This approach can also be seen as a framework for integration of external knowledge with image classification procedures. To evaluate the concept, a software tool has been designed and used for experimentation. The result showed that the per-object maximum likelihood performs much better than the per-pixel method. It led to higher classification accuracy and explicit utilization of the geometrical and topological information about land use objects and land use processes. For generation and testing of the geometric models, the problem of deforestation in Thailand is used.

1 INTRODUCTION

Image segmentation and classification is usually applied at the pixel level (using solely the radiometric properties of pixels on an individual basis) by processing the data in order to arrive at a meaningful partitioning of the image. Pixel-based segmentation and classification procedures start off with “raw-data” (a set of samples of reflectance values) and end up with a segmented and labeled image. In this process the preliminary features or segments are located in the Remote Sensing (RS) data and then examined for consistency (to find correspondence with real world objects). The major problem with these pixel-based approaches is that there is insufficient information to completely isolate the required objects because of the complexity of the objects and of the object radiation interaction in RS images.

Considerable research has been dedicated to improve the pixel-based segmentation and classification results. For example, "classification accuracy improvement” (Hutchinson, 1982), “knowledge-based image analysis” (Civco, 1989; Mulder and Schutte, 1992; Abkar and Sharifi, 1995), “object-based classification” (Janssen *et al.,* 1990), “integration of algorithms” (Schoenmakers, 1995; Gorte, 1998; Janssen, 1994), “model-based image analysis” (Mulder, 1993), "image understanding” (Kohl and Mundy, 1994), “image fusion” (Förstner and Löcherbach, 1992; Pohl and van Genderen, 1998).

It is therefore clear that the spectral data alone is not adequate for rigorous information extraction from RS images. Combining RS spectral data with other multisource (ancillary) data allows the use of more knowledge, which can improve information extraction. Notwithstanding much effort spent already, an operational and (integrated) analysis method is as yet required to combine (fuse) all this Earth observation data with geo-information systems (GISs) and models to make it useful for a user community that is concerned with mapping, monitoring, managing and modeling the Earth surface (Ehlers, 1991; Wang, 1991; Hahn and Baltsavias, 1998; Baatz, 1999).

In this paper we present a method that allows integration of available data and/or knowledge contained in GIS about objects and processes into the analysis of remotely sensed data through hypothesis driven image analysis and effective representation of knowledge about scene objects, sensor, and sensing processes. The analysis, as such, is guided by expectations from the domain and the analysis starts with a model (at the object level) to partition the image. This model-based classification of objects focuses on the integration of RS and GIS; this is done by shape hypothesis generation using a GIS and evaluation of shape hypotheses and shape parameters in the evidences provided by RS images.

2 DESCRIPTION OF THE METHOD

In this paper a framework is developed that allows a formal integration of information derived about objects and processes in the analysis procedure. This is graphically represented in Fig. 1. In the developed framework, the data and/or knowledge contained in a GIS about terrain objects and processes (e.g. growth, harvest, and development) can be combined with the sensor model and the atmospheric model to optimize information extraction from RS data. The proposed model is based on the probability theory, which enable combining information from different sources with the purpose of classifying each pixel and making probabilistic assessments about the model "parameters" (Fig. 1). The *Bayesian probability theory* is used to describe the uncertainties in the relationship between the observed RS data **d**, the hypothetical class label ω_k, and the model parameters **p**, modeled by the *combined probability* prob(**d**, ω_k, **p**) of all relevant factors in both the data domain and model domain. Here **d** is the collection of remotely sensed multi-spectral data at a fixed time and ω_k are the radiometric classes with k as the number of classes defined by the users (map categories) and **p** is the parameter vector of the pattern model (i.e. the combined atmosphere, scene, and sensor…efects). Therefore, for our purpose, we define Pattern = prob(**d**, ω_k, **p**); see Abkar (1999).

We use the Bayes rule, to find maximum probability prob(ω_k|**d**, **p**) over [(x_i, y_j)] and [$\omega_k(x_i, y_j)$, **p**] from (RS) data given the GIS under certain conditions of independency, i.e., separable into a radiometric model and a geometric model.

$$\text{prob}(\mathbf{d}, \omega_k, \mathbf{p}) = \text{prob}(\omega_k \,|\mathbf{d}, \mathbf{p})\text{prob}(\mathbf{d}, \mathbf{p}) = \text{prob}(\mathbf{d}|\omega_k, \mathbf{p})\text{prob}(\omega_k, \mathbf{p})$$

Thus, we have

$$\text{prob}(\omega_k \,|\mathbf{d}, \mathbf{p}) = \frac{\text{prob}(\mathbf{d}|\omega_k, \mathbf{p})\text{prob}(\omega_k, \mathbf{p})}{\sum_{k=1}^{K} \text{prob}(\mathbf{d}|\omega_k, \mathbf{p})\text{prob}(\omega_k, \mathbf{p})} \quad (1)$$

The application of (1) in classification and parameter estimation requires knowledge of the combined probabilities prob(ω_k, **p**). However, a form can be obtained through the application of the law of conditional probability

$$\text{prob}(\omega_k, \mathbf{p}) = \text{prob}(\omega_k|\mathbf{p})\text{prob}(\mathbf{p})$$

since prob(**p**) cancels from the numerator and denominator of (1) after substitution, we have

$$\text{prob}(\omega_k \,|\mathbf{d}, \mathbf{p}) = \frac{\text{prob}(\mathbf{d}|\omega_k, \mathbf{p})\text{prob}(\omega_k \,|\mathbf{p})}{\sum_{k=1}^{K} \text{prob}(\mathbf{d}|\omega_k, \mathbf{p})\text{prob}(\omega_k \,|\mathbf{p})} \quad (2)$$

which is the basis for calculation of the maximum probability values for model parameters Abkar (1999).

The method developed for making use of the information/knowledge about objects and processes stored in GIS and other information (sensor) in the analysis procedure is called *Likelihood-Based Segmentation and Classification* (LBSC) of remotely sensed data (Abkar, 1999) and comprises three main processes (Fig. 1):

1. *a radiometric likelihood generator*, which generates likelihood vectors (probability for radiometry given radiometric class) from multi-spectral RS data and a radiometric model for subsequent analysis by segmentation and classification. Store the likelihood vectors in radiometric evidence maps.

   As was noted that for the proper application of the refined Bayes formula (2), an estimate of prob(**d**|ω_k, **p**) was needed in order to find the probability (2), which are estimated from the training sample set. For a given **p** the set of posteriori probabilities prob(ω_k|**d**) can be arranged to form the K-dimensional *vector* **E** which we referred to as *radiometric likelihood vectors* or *radiometric evidence vectors* $\mathbf{E} = [\text{prob}(\omega_1|\mathbf{d}) \quad \text{prob}(\omega_2|\mathbf{d}) \quad \ldots \quad \text{prob}(\omega_K|\mathbf{d})]^T$.

2. *a geometric hypothesis generator*, which generates geometric hypotheses for image partitioning given initial parameters and with geometric constraints. Current GIS is used as the source of object models to generate geometric hypotheses (Fig. 1). Include the signal mixture model as defined by a sensors point-spread function. Store each iteration over the geometric parameter space in a probability for class vector hypothesis map.

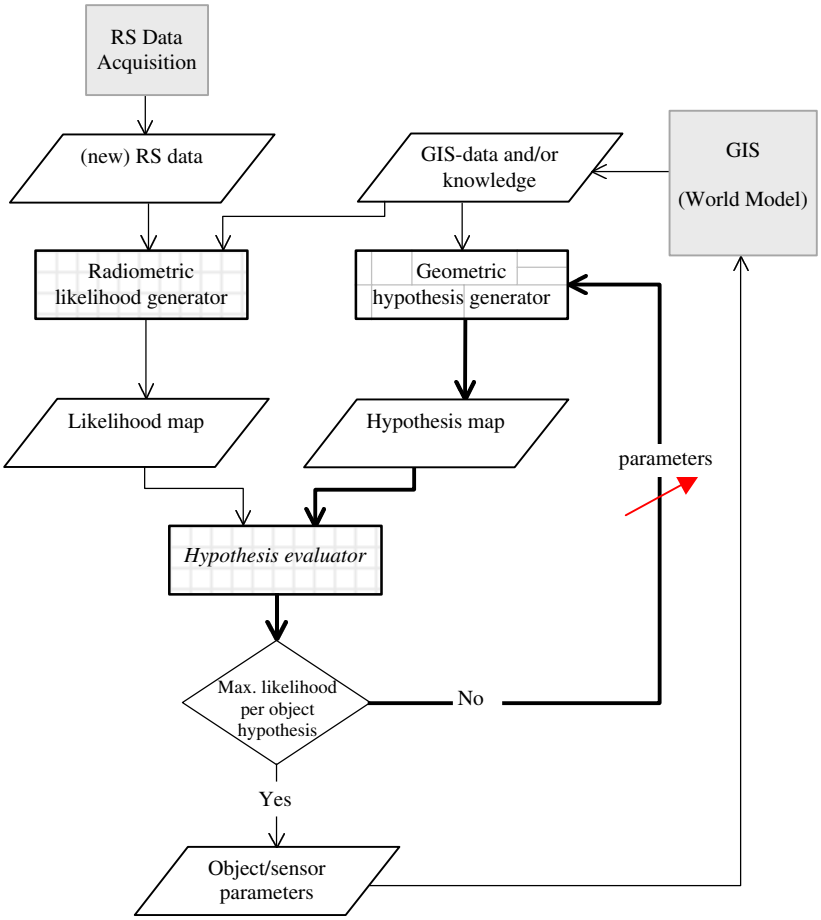

Figure 1. Conceptual representation of likelihood-based segmentation and classification method. In this Figure, processes are represented by rectangles and the obtained information (data sets) are represented by parallelogram.

3. *a hypothesis evaluator*, which evaluates each iteration of the hypothesis generation process calculating the degree of agreement or disagreement between the evidence map and the hypothesis map. This results in the average likelihood over all classes and all objects. When multiplied with a cost/benefit matrix a monetary utility function is produced.
   - If the utility is maximum then stop and update the GIS.
   - If the utility is less than maximum, then change the model (parameters) and go to step 2 and generate new geometric hypotheses maps.

A typical feature of the method is the separation of the complex combined probabilities of multi-spectral data, object class, object geometry, sensors and sensing into a radiometric model and a geometric model. Bayesian inversion of the radiometric model leads to radiometric evidence maps. The geometric hypotheses maps are generated from parameterized object models. Geometric models are constrained by fixed objects and they include elements from the sensor model, such as the point-spread function and the mapping of three-dimensional scenes into two dimensional sample grids. The utility function consists, for each iteration of geometric hypotheses generation, of the matrix over the crossing of all evidence vectors and all hypotheses vectors. This "confusion" matrix is multiplied (inner product) with a benefit/cost matrix. The user of the combined RS&GIS system can optimize the results either in the likelihood domain (unit cost/benefit matrix) or use several different cost/benefit scenarios. Residual error maps show the distribution of residual errors. Study of the utility(parameter) function gives the overall quality in the minimum value of utility.

3. EXPERIMENTATION, VERIFICATION AND EVALUATION OF THE FRAMEWORK

The LBSC is applied to the problem of identifying and estimating the expansion or depletion of forest in the study area located in Thailand from 1977 to 1989 with the use of satellite remote sensing data, such as Landsat-TM images.

3.1 Study Area and Data

The district of Phrao in Chiang Mai province in the northern region of Thailand was selected as a relevant study area. The general landscape is hilly and mountainous surrounding a small lowland area where settlements and agriculture are

concentrated. Deforestation in the district is caused mainly by the expansion of agricultural activities and fuelwood gathering of the lowland population (Ato, 1996).

The following RS and GIS data were used for the procedure of image analysis:

- The Phrao Landsat-TM obtained on February 1989 (Fig. 2-a);
- Land use/cover map of 1989 (Fig. 2-b), which serves two purposes:
  - Training field selection for generation of the radiometric likelihood vectors.
  - Evaluation of the classification results.
- Land use/cover map of 1977; derived from digitization on the aerial photograph of 1977 (Fig. 2-c),
- Soil map at a scale of 1:100,000 obtained from the Dept. of Land Development in Chiang Mai, Thailand (Fig. 2-d);

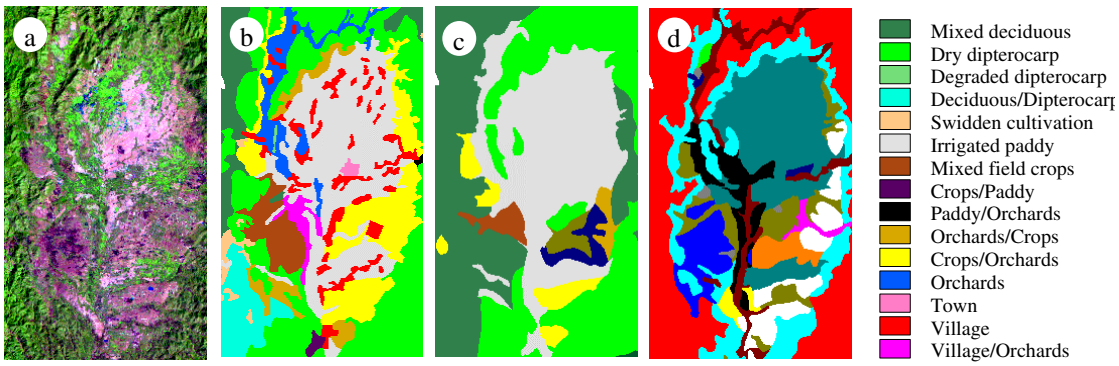

Figure 2. TM image & reference maps of Phrao District, Chiang Mai Province, Thailand
(a) TM image of Phrao District; natural color composite of Band 5, 4, and 3 (RGB); image size: 402 cols × 700 rows.
(b) Land use/cover map of 1989 including 15 generalized land cover classes (4 forest and 11 non-forest classes)
(c) Land use/cover map of 1977
(d) Soil map of Phrao District at a scale of 1:100,000

3.2 Radiometric Likelihood Generator

In the case of the maximum likelihood per-pixel algorithm the class to which the pixel is finally assigned is that with the highest probability. Probabilities of class membership, on which the assignment is based, are usually disregarded so that after classification no information on the probabilities is available. In order to overcome the limitations of the classical techniques, such as maximum likelihood classification per-pixel, the "images" are mapped into the likelihood of class labels per sample under the assumption of equal prior probabilities. It is assumed that the normal distribution function will approximate the frequency distribution associated with each of the classes.

The likelihood vectors are stored in radiometric likelihood maps. The likelihood maps or evidence maps show the probabilities that a sample belongs to each of the defined set of possible land cover classes, obtained by supervised classification of the multi-band satellite images. Because of the interest in the boundary between forest and non-forest, we have combined all the forest likelihood maps in one likelihood map for forest shown, in Fig. 3-a, and all non-forest likelihood maps in one likelihood map for non-forest, which is shown in Fig. 3-b.

3.3 Geometric Hypothesis Generator

In this section, the available data and/or knowledge contained in the GIS database about the shape of forest and non-forest objects and processes will be used to predict the RS data about the extent of deforestation (expansion of the non-forest area) in the study area by shape hypotheses generation. By using a parameterized class membership function, geometric knowledge is represented in parameterized models resulting in a hypothesis map. The hypothesis map depends on a geometrical object model with morphological parameters.

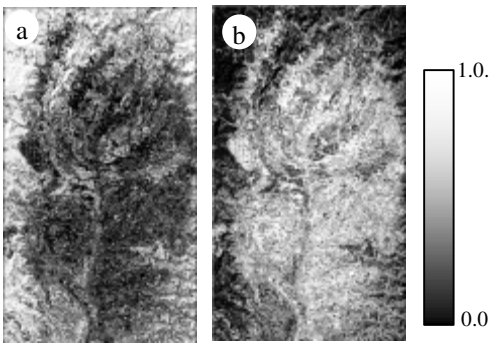

Figure 3. Forest and non-forest likelihood maps
a) likelihood map for forest class
b) likelihood map for non-forest class.

Various models of hypothesis generation using Landsat-TM images and GIS data and knowledge are tested. The assumption that deforestation starts from existing agricultural lands (non-forest classes) and spreads out towards forest areas guide the authors toward the use of morphological model for the expansion

of agricultural areas and the process of deforestation. Two main approaches for hypothesis generation about the shape of forest/non-forest objects are:

First, in the absence of GIS data, a method of automatic shape hypothesis generation of RS data by means of local maximum likelihood (LML) classification is used as a shape hypothesis generator for LBSC (Abkar 1999). Fig. 4-b shows the forest and non-forest cover map obtained from the automatic shape hypothesis generator by means of LML classification of the 1989 TM image, which contains small-patched and sparsely distributed deforested areas.

Second, based on the availability of data and/or knowledge from the GIS the initial hypothesis with an irregular shape was generated. Rules for the development and change of the irregularly shaped forest/non-forest objects from simple morphological parameters are formulated to generate shape hypotheses. After which the parameters are determined based on the RS data. Given an initial state of non-forest class (or forest cover) the "isotropic expand" operation is used to predict the next state of the non-forest class (see Fig. 5). The expand hypothesis is parameterized by using the number of successive "pixel" expands applied to the reference map of 1977. Isotropic expansion is selected optionally as 4 nearest neighbor expansion.

The assumption underlying the isotropic expand operation (people cut trees at the forest boundary at the same rate), was not reasonable, as appeared in the (residual) error maps, with error patterns indicating an incomplete geometric hypothesis. Adding constraints such as soil to the deforestation process significantly improved the isotropic expansion of the non-forest area (see Fig. 6). The soil map is resampled to the coordinate system of the Landsat-TM sensor (Fig. 2-d) and then the soil suitability map for agriculture is derived. Next, this constraint map, are crossed with the deforestation hypothesis map to generate constraint hypothesis maps. Therefore, the prior knowledge in this case, consists of an initial state represented in a reference map of 1977 and the underlying assumption for the generation process is the process of expansion constrained by, for example, soil and land form. This is called "soil-constrained isotropic expand" but the generated constraint hypotheses maps are non-isotropic, i.e. the generated result is non-isotropic (e.g. Fig. 6-b).

Using global geometric hypothesis such as unconstraint and soil constraint isotropic expends have the disadvantages that the generated hypothesis boundaries are artificial and cannot account for local changes. Consequently, the method of isotropic and soil-constrained isotropic expands were extended to "non-isotropic expand" by using local radiometric constraints for application of expand in the framework of hypothesis generation and parameter estimation; this is in contrast with the pixel-based approaches. The method is capable of dealing with regular, irregular and small-patched and sparsely distributed deforested areas (Fig. 7).

3.4 Hypothesis Evaluation & Error Analysis

In this section the model results are evaluated by the minimum cost solution of hypotheses. The graph of the cost function and the representation of the residual error maps are used for the evaluation of the model to measure the outcomes from the geometric hypotheses. Then, the results are evaluated by the minimum cost solution of hypotheses. Figures 4-b, 5-b, 6-b, and 7-b show the forest and non-forest cover map obtained from the various models of hypothesis generation using Landsat-TM images and GIS data and knowledge. The graphs of the costs are also shown in Figures 4-a, 5-a, 6-a, and 7-a. The deforestation maps can be determined by comparing the classification results with the land use/cover map of 1997 (see Figures 4-c, 5-c, 6-c, and 7-c).

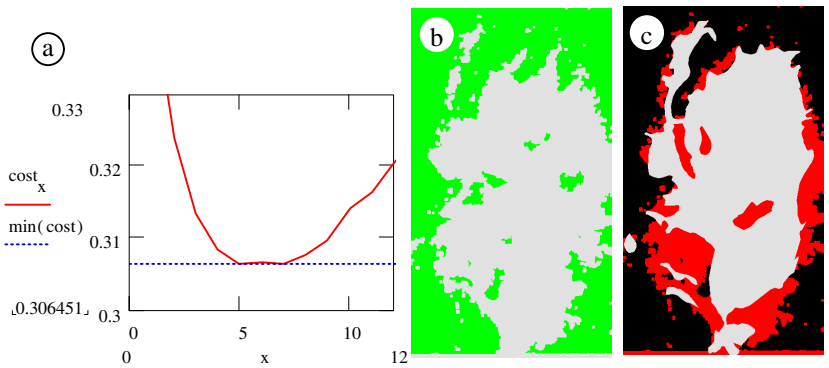

Figure 4. Forest and non-forest cover map obtained from the automatic shape hypothesis generator.
(a) the graph of the cost as a function of the number of shrink operations (Local min) for LML classification. The graph has a min-cost of 0.306451 at Local-min-parameter = 8.
(b) the best result of the LML classification
(c) deforestation map of Phrao between 1977 and 1989.

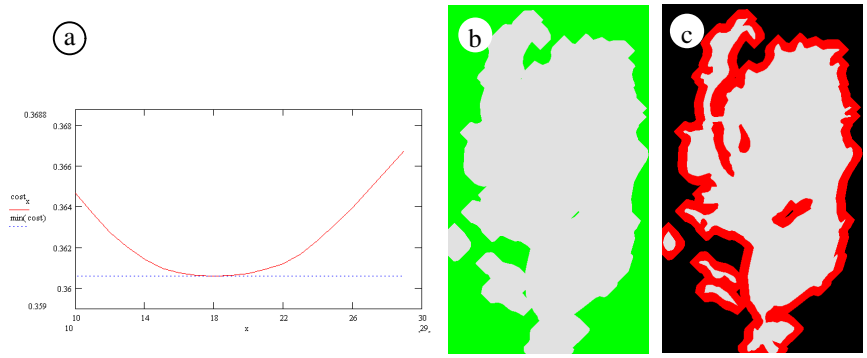

Figure 5. Forest and non-forest cover map obtained by the isotropic expand hypothesis generation.
(a) the graph of the cost as a function of the number of expand operations in case the land use map of 1977 is used for expansion. It has a min-cost of 0.360612 at expand-parameter=18.
(b) the best result of the iterative isotropic expand operations for i = 18
(c) deforestation map of Phrao between 1977 and 1989 using isotropic expand operations.

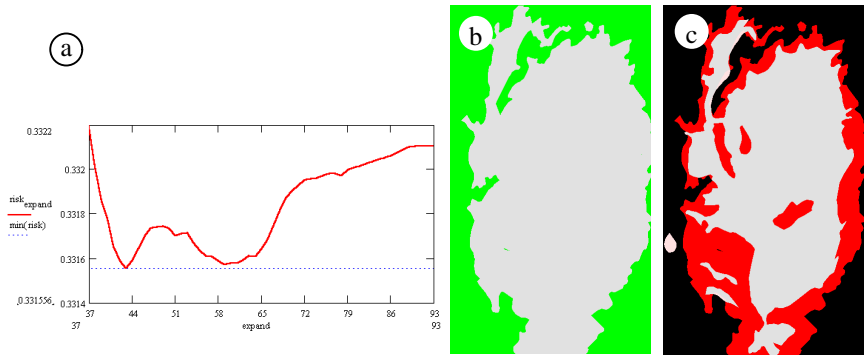

Figure 6. Forest and non-forest cover map obtained by the soil-constrained isotropic expand hypothesis generation.
(a) the graph of the cost as a function of the number of expand operations. The graph has a min-cost of 0.331556 at soil-constrained-expand-parameter = 44.
(b) the result of the non-isotropic expand operations for i = 44.
(c) deforestation map of Phrao between 1977 and 1989 on the basis of the soil-constrained isotropic expand result.

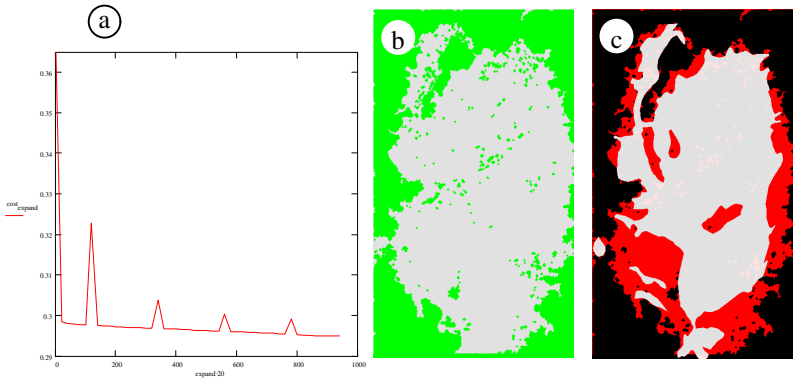

Figure 7. Forest and non-forest cover map obtained by the non-isotropic expand with the use of the seed objects from the land use map of 1977.
(a) the graph of the cost as a function of the number of conditional expand operations (*N* cond. Dilation for *N*= 0...900). The graph has a minimum cost of 0.295039 at N = 801.
(b) the best result of the non-isotropic expand
(c) deforestation map of Phrao between 1977 and 1989 on the basis of the non-isotropic expand result.

3.5 Overall Evaluation of Results

The resulting minimum costs of error solutions are compared with classical methods of image classification based on per-pixel maximum likelihood (ML) classification followed by merging based on majority operators. The results of the ML classification are shown in Fig. 8.

The available reference land use map of 1989 (ground truth) is also used to create the confusion matrices, in order to assess the accuracy of the classified results. The reference data is used to check whether the result of the model comes close to a man-made interpretation of the non-forest area, notwithstanding the errors made in man-made interpretations of the ground truth map—the ground reference data (or ground truth) cannot be regarded as the absolute truth.

However, for comparison of the model results with the improved ML classification result, a 3×3 Majority filter is applied (8 times) to the result of ML classification to smooth the classified result (Table 1).

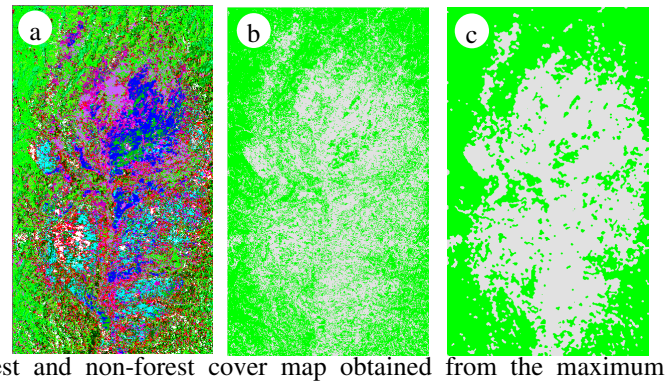

Figure 8. Forest and non-forest cover map obtained from the maximum likelihood per-pixel classification of the Phrao Landsat-TM image of 1989.
(a) with 19 land cover classes
(b) with two merged land cover classes (forest and non-forest)
(c) after 8 applications of the majority filter. To treat isolated and mixed pixels, a post-merging operator is applied to the ML result, iteratively.

Methods	Overall accuracy %
ML classification	69.39
Filtering results	80.21
LML classification	83.93
Isotropic expand	86.29
Non-isotropic expand (likelihood-based constrained expend)	87.09
Soil-constrained isotropic expand	88.70

Table 1. Accuracy assessment of the various models for hypothesis generation

4. CONCLUSIONS

In this paper a Likelihood-Based Segmentation and Classification method (LBSC) for remotely sensed images, with ultimate goal of describing objects in terms of their positions, sizes, shapes and geometric relations, based on a minimum-cost or maximum-benefit principle. A key feature of the LBSC method is to break down the image analysis into an evidence part and a hypothesis part; the evidence part comes from the RS data and the hypothesis part comes from the analyst knowledge which might have been stored in GIS. RS and pattern classification provide evidence (likelihood vectors) for subsequent analysis by segmentation and classification. Hypothesis evaluation provides a cost/benefit optimization criterion for finding the best hypothesis to match the evidence using the cost matrix, which is user specific. In this way the objectives and preferences of users/decision-makers are taken into account. The model parameters are adjusted until there is a minimum cost (or maximum benefit) value for the hypotheses and parameters. Therefore, instead of maximum a posteriori probability for each image sample (pixel), maximum a posteriori probability per object hypothesis and object parameters is derived. In other words, minimum cost of confusion per object over all objects and data samples is derived.

In summary, the experimental results indicated the following main achievements:

- A new method of image segmentation and classification to estimate the geometry and radiometry of objects using remotely sensed data.
- A framework for integration of prior/external knowledge (GIS) in image analysis, which is based on the combined probability of RS data and object models for the entire sample set of RS data by hypothesis generation and parameter estimation with a Bayes type cost/benefit function, which allows:
  - generation and prediction of the initial shape hypotheses of objects, and if relevant, incorporate constraints in hypotheses generation process
  - perform per-object segmentation and classification;
  - perform calculation of per-object accuracy (maximum likelihood per-object hypothesis);
  - derivation of the shape description of objects;
  - Provide a formal framework for application of available knowledge/information of objects in classification process.
- Extension of the geometric model to objects of non-rectangular shape, i.e. the algorithm can create irregularly shaped segments; this makes the approach applicable to various cases.

REFERENCES

Abkar, A.A., 1999. Likelihood-Based Segmentation and Classification of remotely sensed images - A Bayesian Optimisation Approach for Combining RS and GIS. PhD Thesis, University of Twente, Enschsde, The Netherlands, ISBN 90-6164-169-1, ITC publication number 73.

Abkar, A. A. and Sharifi, M. A., 1995. Knowledge-Based Classification Method for Mapping of Land Cover Using High Resolution Satellite Data. *Proceedings of the 1st Conference on Space Technology and Developing Countries*, Iranian Research Organization for Science and Technology, Tehran, Iran, STC-95-143: 1-19.

Abkar, A. A. and Mulder, N. J. 1998. Likelihood-Based Classification of High Resolution Images to Generate the Initial Topology and Geometry of Land Cover Segments. *Proceedings ISPRS Commission IV: GIS Between Visions and Applications*, The International Archives of Photogrammetry and Remote Sensing, Volume XXXII, Part 4, Stuttgart, Germany.

Ato, V. A., 1996. Prediction of Deforestation Using Area Production Model and GIS, A Case Study of Phrao, Chiangmai, Thailand. MSc. Thesis, ITC, Enschede, The Netherlands.

Baatz, M., 1999. Delphi2 Creative Technologies GmbH, Germany: object-oriented and Multi-scale image analysis in semantic networks. 2nd International Symposium on Operationalization of Remote Sensing, August 16-20, ITC, Enschede, The Netherlands.

Civco, D., 1989. Knowledge-Based Land Use and Land Cover Mapping. *Proceedings of Annual Convention of American Society for Photogrammetry and Remote Sensing, Vol. 3,* 276-291, Baltimore, Maryland.

Ehlers, M., Greenlee, D., Smith, T. and Star, J., 1991. Integration of Remote Sensing and GIS: Data and Data Access. *Photogrammetric Engineering & Remote Sensing Vol. 57, No. 6,* 669-675.

Förstner, W. and Löcherbach, T., 1992. Fusing Information in Remote Sensing. *ISPRS* Congress, Commission III, Washington.

Gorte, B., 1998. Probabilistic Segmentation of Remotely Sensed Images. Ph.D. Thesis Wageningen Agricultural University (WAU), ITC, Enschede, The Netherlands, ISBN 90-6164-157-8, ITC Publication 63.

Hahn, M. and Baltsavias, E., 1998. Cooperative Algorithms and Techniques of Image Analysis and GIS. *Proceedings ISPRS Commission IV: GIS Between Visions and Applications*, The International Archives of Photogrammetry and Remote Sensing, Volume XXXII, Part 4, Stuttgart, Germany.

Hutchinson, C., 1982. Techniques for Combining Landsat and Ancillary Data for Digital Classification Improvement. *Photogrammetry Engineering and Remote Sensing, Vol.48, No. 1,* 123-130.

Janssen, L. L. F., 1994. Methodology for Updating Terrain Object Data from Remote Sensing Data; The Application of Landsat TM Data with Respect to Agricultural Fields. Doctoral thesis, Wageningen Agricultural University, Wageningen, The Netherlands.

Kohl and Mundy, 1994. The Development of the Image Understanding Environment. *Proceedings of the Conference on Computer Vision and Pattern Recognition,* pp 443-448, Seattle, WA.

Mulder, N. J., Abkar, A. A., 1999. A Comparison of Least Squares and Bayesian Minimum Risk Edge Parameter Estimation. *Pattern Recognition Letters 20 (1999) 1397-1405.*

Mulder, N. J., 1993. A theory of Geoinformatics with a sub-theory for image analysis of RS data, the integration of GIS and RS, model based image analysis. *Proceedings of Intern. Geoscience and RS Symposium (IGARSS'93),* Tokyo, Vol. IV, 1883-1885.

Mulder, N. J. and Schutte, K., 1992. Knowledge Engineering in RS and Knowledge Based System in GIS. *Proceedings ISPRS Washington D.C. ISSN 0256-1840, Vol. 3*, 965-968.

Pohl, C. and van Genderen, J. L., 1998. Review Article, Multisensor Image Fusion in Remote Sensing: Concepts, Methods and Applications. *International Journal of Remote Sensing, Vol. 19, No. 5*, 823-854.

Richards, J. A., 1999. *Remote Sensing Digital Image Analysis: An Introduction.* Third Revised and Enlarged Edition, Springer-Verlag, Heidelberg, Germany.

Schoenmakers, R. P. H. M., 1995. Integrated Methodology for Segmentation of Large Satellite Images in Land Applications of Remote Sensing. Ph.D. Thesis, JRC, Italy.

Sharifi, M. A., van Keulen, H., Driessen, P., Bronsveld, M. C., Clavaux, M. B. W, Leenaard, J., and Dehghan, A., 1999. Development of crop inventory and forecasting system for the major agricultural commodities in Hamadan Province Islamic Republic of Iran. Final Report, ITC publication.

Wang, F., 1991. Integrating GIS's and Remote Sensing Image Analysis Systems by Unifying Knowledge Representation Schemes. *IEEE Transactions on Geoscience and Remote Sensing, Vol. 29, No. 4,* 656-664.